

Substituting Coumarins for Quinolinones: Altering the Cycloreversion Potential Energy Landscape

Nicholas Paul,[†] Man Jiang,^{†,§} Nikolai Bieniek,[‡] J. Luis Pérez Lustres,[†] Yang Li,[†] Nikolaus Wollscheid,[†] Tiago Buckup,[†] Andreas Dreuw,[§] Norbert Hampp,^{*,‡,§} and Marcus Motzkus^{*,†}

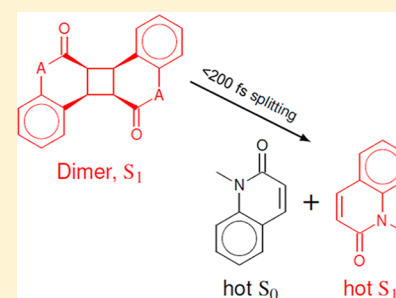
[†]Physikalisch-Chemisches Institut, Im Neuenheimer Feld 229, 69120 Heidelberg, Germany

[§]Interdisziplinäres Zentrum für Wissenschaftliches Rechnen und Physikalisch-Chemisches Institut, Ruprecht-Karls Universität, Im Neuenheimer Feld 205, 69120 Heidelberg, Germany

[‡]Fachbereich Chemie, Philipps-Universität Marburg, Hans-Meerwein-Straße 4, 35032 Marburg, Germany

Supporting Information

ABSTRACT: The light-activated cleavage of cyclobutane-based systems via [2 + 2] cycloreversions, such as thymine and coumarin dimers, is an important but still poorly understood ultrafast photochemical reaction. Systems displaying reversible cycloreversion have found various uses in cross-linked polymers, enhancing gas adsorption affinities in inorganics, and light-activated medical therapies. We report the identification of a heterogeneous mode of cycloreversion for a rarely examined coumarin analogue system. Quinolinone monomers and dimers were probed using ultraviolet pumped, transient absorption spectroscopy and demonstrated radically different photophysical properties than coumarins. Monomers displayed enhanced intersystem crossing at almost 1:1 versus the combined nonradiative and radiative singlet decay, while the dimers underwent cycloreversion to a one excited—one ground state monomer photoproduct pair. The change in both systems was directly linked to the lactame group in the quinolinone motif. This discovery highlights the dramatic effects that small chemical changes can have on photoreaction pathways and opens up a new means to produce and develop more efficient cycloaddition–cycloreversion systems.



The change in both systems was directly linked to the lactame group in the quinolinone motif. This discovery highlights the dramatic effects that small chemical changes can have on photoreaction pathways and opens up a new means to produce and develop more efficient cycloaddition–cycloreversion systems.

INTRODUCTION

Chemical transformations, such as bond dissociation,^{1,2} internal conversion,³ isomerization,⁴ torsional relaxation,⁵ and tautomerization,⁶ are just a few of the many possible routes of photoinduced molecular excited state decay. Exposure of molecules to ultraviolet (UV) light, due in part to the high photon energy, typically provides more possible routes for chemical transformation than in thermal ground state chemistry. This, however, can lead to the inherent problem of molecular instability and also can be more prominent,⁷ particularly for organic materials.⁸ One prominent example is the thymine–thymine dimer formation which is a key mechanism of UV-induced photodamage in DNA.⁹ However, there are various instances where UV irradiation can lead to productive or nondetrimental photophysical processes. Within the same thymine–thymine dimer example just given, it has been suggested that the DNA dimer formation may actually participate in methods of DNA photoprotection.¹⁰ Much ambiguity still remains regarding the influence of light, particularly UV light, on molecular systems; nonetheless, there are many research avenues that look to remove such ambiguity. In applied research, photochromic molecular switches sensitive in the visible-UV region, which behave similarly to the DNA dimerization mentioned, have found applications in optoelectronic devices.^{11–13} Photochromic systems also found use in optically triggered, medical

applications, relevant examples being the use of coumarin dimer-based compounds in photodynamic therapy for controlled drug release^{14–17} and the treatment of eye cataracts.¹⁸

Further development of technologies centered around photoinduced molecular reactions and rearrangements requires deeper understanding of the underlying physical mechanisms involved. Previous research on coumarin dimer photocleavage addressed the stereochemical influence on the ring cleavage efficiency.¹⁹ Furthermore, the effects of single- and two-photon absorption,^{16,20,21} solvent dependence,^{22,23} and functional group influence on the ring cleavage efficiency and mechanism^{14,24} have been investigated. In this paper, we aim to understand the structure–function relationship behind [2 + 2] cycloreversions by investigating a different class of molecules closely related to the classically studied coumarin systems. Quinolinones are the lactame analogue of coumarins (Figure 1A),²⁵ which also have various applications in medical treatments.^{26–29} The irradiation of both coumarin and quinolinone dimer systems yields a typical $\pi\pi^*$ excited electronic state, which is located primarily across the phenyl and carbonyl groups of each monomer unit. Therefore, we

Received: July 26, 2018

Revised: August 30, 2018

Published: September 5, 2018

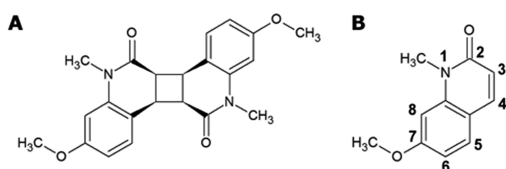


Figure 1. (A) Molecular structure of the *syn*-ht quinolinone dimer stereoisomer. (B) Molecular structure of the corresponding quinolinone monomer (7-methoxy-1-methylquinolin-2(1H)-one). The structure has been numbered to show the standard IUPAC numbering for this molecular motif.

expect to induce a noticeable change in the ring cleavage process when substituting the more electronegative oxygen in coumarin for a nitrogen in the quinolinone. The results of the study used the same UV pump–visible probe transient absorption technique as used for the previous study of coumarin dimer stereoisomers.¹⁹ Additionally, we also studied and characterized the quinolinone monomer (Figure 1B). Analysis of the resulting data showed substantial differences in both the quinolinone monomer and dimer compared to the related coumarins. The lactone to lactame functional group substitution not only contributed primarily to increased fluorescence of the quinolinone monomer (compared to coumarin monomers), but it also substantially altered the dimer ring cleavage mechanism. The results to be presented and discussed give strong evidence as to the ability of changing the nature of the ring-cleaved, monomer photoproducts formed. Lactone to lactame substitution switched the product formation from a homogeneous pair of monomers in a thermally hot ground state to a heterogeneous, one ground–one excited singlet state monomer product pair.

EXPERIMENTAL SECTION

Materials for Molecular and Ring Cleavage Quantum Yield Studies. Methyl iodide (99%, Alfa Aesar), sodium hydride (60% suspension in paraffin wax, Sigma-Aldrich), *meta*-anisidine (98%, Alfa Aesar), cinnamoyl chloride (98%, Acros Organics), aluminum chloride (purum, Merck), dimethylformamide (purum, Acros Organics), dichloromethane (99.8%, Acros Organics), magnesium sulfate (p.a., Sigma-Aldrich), and sodium chloride (tec. Sigma-Aldrich) were used as received. Dichloromethane and acetonitrile (99.9% Acros Organics) were used for photochemical reactions. Acetonitrile for analytic HPLC measurements was gradient grade (VWR Chemicals); for all other experiments solvents were of technical quality and purified by distillation prior to use.

Preparation of 7-Hydroxyquinolin-2(1H)-one. 7-Hydroxyquinolin-2(1H)-one was prepared following a literature procedure.³⁰ Yield: 64%. ¹H NMR (300 MHz, dimethyl sulfoxide-*d*₆): δ /ppm = 6.21 (d, ³J = 9.1 Hz, 1H, CH), 6.62 (d, ³J = 8.5 Hz, 1H, CH), 6.69 (d, ³J = 2.2 Hz, 1H, CH), 7.44 (d, ³J = 8.5 Hz, 1H, CH), 7.73 (d, ³J = 9.4 Hz, 1H, CH), 10.08 (s, 1H, OH), 11.48 (s, 1H, NH).

Preparation of 7-Methoxy-1-methylquinolin-2(1H)-one. 7-Hydroxyquinolin-2(1H)-one (9.29 g, 0.06 mol) was suspended in 80 mL of dimethylformamide under inert conditions. The suspension was cooled to 0 °C, and sodium hydride (60% suspension in paraffin wax, 4.88 g, 0.12 mol, 2.2 equiv) was slowly added. The suspension was stirred for 15 min followed by dropwise addition of methyl iodide (7.5 mL, 0.12 mol, 2.1 equiv). The reaction vessel was stirred for 1 h

and the solvent removed under reduced pressure. The remaining solid sample was dissolved in ethyl acetate followed by extraction with water and brine. The organic layer was dried over magnesium sulfate and the solvent removed under reduced pressure. The solid sample was recrystallized from dichloromethane giving 4.96 g (0.03 mol, 45%) of the solid 7-methoxy-1-methylquinolin-2(1H)-one product. ¹H NMR (300 MHz, dimethyl sulfoxide-*d*₆): δ /ppm = 3.60 (s, 3H, O–CH₃), 3.90 (s, 3H, N–CH₃), 6.42 (d, ³J = 9.4 Hz, 1H, CH), 6.92 (dd, ³J = 15.2 Hz/6.5 Hz, 2H, 2 × CH), 7.63 (d, ³J = 8.6 Hz, 1H, CH), 7.81 (d, ³J = 9.4 Hz, 1H, CH). HRMS (ESI+) *m/z* = calc. (M⁺ + Na⁺): 212.0682; found: 212.0681.

Preparation of *syn*-Head-to-Tail 7-Methoxy-1-methylquinolin-2(1H)-one Dimer. 7-Methoxy-1-methylquinolin-2(1H)-one (8.54 g, 0.05 mol) was dissolved in 100 mL of dried and degassed acetonitrile. The reaction vessel was irradiated in the photoreactor for 48 h. The formed precipitate was filtered off and washed with methanol leaving 2.12 g (5.6 mmol, 25%) of the solid *syn*-head-to-tail 7-methoxy-1-methylquinolin-2(1H)-one dimer product. ¹H NMR (500 MHz, dimethyl sulfoxide-*d*₆): δ /ppm = 3.44 (s, 6H, 2 × O–CH₃), 3.71 (m, 4H, 4 × CH_{cyclobutane}), 3.83 (s, 6H, 2 × N–CH₃), 6.53 (d, ³J = 8.2 Hz, 2H, 2 × CH), 6.59 (s, 2H, 2 × CH), 6.84 (d, ³J = 8.2 Hz, 2H, 2 × CH). HRMS (ESI+) *m/z* = calc. (M⁺ + Na⁺): 401.1472; found: 401.1462.

Dimerization Reactions. The dimerization reactions were performed in an air-cooled Rayonet-type photoreactor equipped with 16 Osram Eversun 40 W/79K UV fluorescent tubes ($\lambda_{\text{max}} = 350$ nm). The reaction process was monitored via HPLC performed on an Ultimate 3000 system (Dionex) equipped with a diode array detector. An RP-18 column was used with a 75:25 (v/v) mixture of acetonitrile and water as an eluent.

NMR Spectroscopy. ¹H NMR spectra were measured on an AV-300 (300 MHz, Bruker), respectively, and AV-500 (500 MHz, Bruker) for the dimers. Dimethyl sulfoxide-*d*₆ was used as solvent. The δ chemical shift scale was calibrated using the residual solvent peak.

Steady-State Spectroscopic Characterization and Fluorescence Quantum Yield Estimation. UV/vis spectra of the samples were recorded on a Cary 100 (Agilent Technologies) spectrophotometer. Photoluminescence spectra were recorded with a Varian Cary Eclipse (Agilent Technologies). The fluorescent standard used was Coumarin 120 in the same solvent, acetonitrile. Anhydrous grade acetonitrile was used and extracted from the solvent container under a strong nitrogen purge. Samples were measured using an ultramicrom quartz cuvette with 2 mm path length (105.250-15-40, Hellma-Analytix) for both absorption and fluorescence measurements.

Determination of the Quantum Yield of the *syn*-Head-to-Tail 7-Methoxy-1-methylquinolin-2(1H)-one Dimer. The cycloreversion reaction of the quinolinone dimer to monomer photoproducts was monitored and analyzed using UV/vis-spectroscopy. UV/vis spectra of the samples were recorded on a Lambda 35 spectrophotometer (PerkinElmer). The quinolinone solution in acetonitrile was irradiated using a UV-LED ($\lambda = 265$ nm; Thorlabs). The light intensity was determined using a photodiode (S1337-1010BQ, Hamamatsu). The irradiated sample area was kept constant using a cover, and the sample was stirred throughout the experiments.

Femtosecond Transient Absorption Experiments. The setup used was based on a tunable UV pump source and a broadband supercontinuum for the wavelength selective probing. As a light source, a regenerative Ti:sapphire amplifier system (CPA 1000, Clark-MXR, Inc.) was used to deliver 800 nm pulses with 640 μJ per pulse and a repetition rate of 1 kHz. To generate UV pump pulses, 300 μJ of the fundamental 800 nm was used to pump a two-stage nonlinear optical parametric amplifier (NOPA) generating visible pulses.^{31,32} The visible pulses were overcompressed by a pair of fused silica prisms in order to compensate for all dispersive optical elements after the second harmonic crystal for UV generation, which has been described previously.^{33,34} After compression, the visible pulses were frequency doubled in a BBO crystal with 55 μm thickness, generating an excitation spectrum with a tunable range from 250 to 300 nm. For excitation of the dimers, the pump wavelength was tuned to 280 or 320 nm. The pump pulses were characterized using a home-built two-photon absorption autocorrelation with a photomultiplier tube (9423B, ET Enterprises). The pulse duration was determined to be less than 30 fs for the whole tunable UV range (250–300 nm). A single filament supercontinuum pumped by 800 nm served as the probe light, which spans most of the visible range and extends to the UV around 300 nm. Such a broad continuum was generated in a 5 mm CaF_2 plate, which was mounted and circularly translated using a motor-driven stage, in order to minimize optically induced damages. After interaction with the sample, the probe light was dispersed by a prism-based spectrograph which gives a detection range from 300 to 650 nm. The spectrally resolved intensity of each laser shot was recorded by a homemade multichannel photodiode array. The time resolution of the measurements was, optimally, about 60–70 fs. All measurements were carried out at magic angle (54.71°) between pump and probe polarizations.

Quinolinone monomer and dimers were diluted in acetonitrile in a 350 μm quartz windowed optical flow cell. The optical density of each sample was adjusted to be nearly the same value of about 0.3 at the corresponding pump wavelength.

Nanosecond Transient Absorption Experiments. The transient absorption measurements were performed with a Helios Fire Setup from Ultrafast Systems. Briefly, fundamental pulses were derived from a Ti:Sa regeneratively amplified laser system (Coherent Astrella). The system delivers 90 fs pulses with 1.5 mJ energy at 4 kHz repetition rate. About 0.650 mJ was used for pumping a commercial parametric oscillator (TOPAS, Light Conversion), by means of which the pump beam was generated. The latter was tuned to 280 nm and was obtained by second harmonic generation of a pump + idler sum frequency beam. The sample was excited with 200 nJ and an approximate spot size of 0.3 mm. Part of the fundamental beam was focused onto a CaF_2 plate for white-light generation. The white light was collected, parallelized, and imaged onto the sample cell with a set of parabolic mirrors. Signal and reference beams are registered by independent spectrographs at 4 kHz repetition rate. The transient absorption signal was averaged for 1 s and the final signal results from three independent scans. The continuum was unpolarized and covers a spectral window ranging from 350 to 650 nm. Pump–probe delays up to 8 ns were scanned with an optical delay line with an instrument response function of 100 fs. Longer delays (up to 400 μs) are accessible with the help of a low-timing-jitter supercontinuum laser (EOS, Ultrafast Systems), which is

electronically delayed with respect to the pump pulse. In this later case, the instrument response function amounts to >0.1 ns, as it is limited by the pulse duration of the continuum laser and the timing jitter.

For reversible photoinduced processes, the sample was dissolved in acetonitrile and brought into a 2 mm thick fused silica cell (Starna). Typically, an absorption of 0.5 at the excitation wavelength was used. The solution was stirred during measurements. For nonreversible photoinduced processes, a 0.2 mm thick fused silica flow cell (Starna) was used. The sample was pumped with a peristaltic pump at a flow rate of 4 mL/min.

Global Analysis of the Transient Absorption Data. Transient absorption data were preprocessed using a combination of a 5×5 moving average filter and SVD to minimize noise contributions to the data (see the [Supporting Information](#)). Coherent artifact was removed by using an acetonitrile solvent background. Transient absorption data were corrected for the chirp of the white-light continuum with the help of the nonresonant coherent solvent signal.³⁵ The resulting transient data were globally fitted with a multi-exponential function and basis functions describing the coherent contribution at early time. The set of exponential functions and decay-associated difference spectra (DADS) were transformed into time-dependent concentrations and evolution-associated difference spectra (EADS) under the assumption of an underlying kinetic model and by assignment of the fitted decay times to microscopic rate constants of the mechanism. All fitting procedures were self-programmed in Matlab R2016a. See the [Supporting Information](#) for further details.

Quantum Chemical Calculations of the Quinolinone Monomer and Dimer Species. To assist in the data analysis, quantum chemical calculations were performed for three model systems. The equilibrium geometries of the quinolinone dimer and monomer ([Figure 1A](#) and [B](#)) were optimized using density functional theory (DFT) with the B3LYP-D3 exchange-correlation functional and the 6-31G* basis set.^{36,37} A quinolinone monomer devoid of the α,β -unsaturated carbonyl group, where only a single bond exists between carbon atoms 3 and 4 (see [Figure 1B](#) for atomic labeling) and the valence sites on each carbon contain a methyl group, was also computationally studied (see [Supporting Information Figure S5](#)). This model compound is representative of the quinolinone dimer cleaved across the cyclobutane ring but maintains the same degree of π -conjugation and is used as a reference for investigating the presence or absence of excitonic coupling within the quinolinone dimer (dubbed reference monomer for the remainder of this paper). Vertical excitation energies were calculated using time-dependent DFT (TDDFT),³⁸ with and without implementation of the Tamm–Dancoff approximation (TDA),³⁹ and in combination with the B3LYP, BHLYP,⁴⁰ and CAM-B3LYP⁴¹ exchange-correlation functionals as well as configuration interaction singles with perturbative doubles (CIS(D))⁴² and the algebraic diagrammatic construction scheme for the polarization propagator at second-order level (ADC(2)).^{43–45} All calculations employed the 6-31G* basis set and were performed using the Q-Chem 5.0 package.⁴⁶

RESULTS

The quinolinone dimer in question ([Figure 1A](#)) undergoes cycloreversion across the cyclobutane ring to yield two

quinolinone monomer units (Figure 1B). The dimer and monomer contain the same hydrocarbon σ -bond manifold, with the obvious differences at the carbon positions where the bridging cyclobutane ring exists in the dimer but not in the monomer. However, as can be seen in Figure 1, the π -system differs, with an extra C=C double bond across the carbon 3 and 4 positions in the case of the monomer. This typical monomer–dimer structural relationship, and nomenclature, is customary in systems that undergo cycloreversion and cycloaddition. The main results will be discussed in the following order: steady-state spectroscopic characterization, density functional theory, and finally time-resolved spectroscopic experiments. Extra figures, including all raw transient absorption data, are given in the Supporting Information.

Steady-State Absorption Spectra, Photoluminescence, and 2D NMR Characterization. Absorption spectra for both the dimer and the monomer are given in Figure 2A

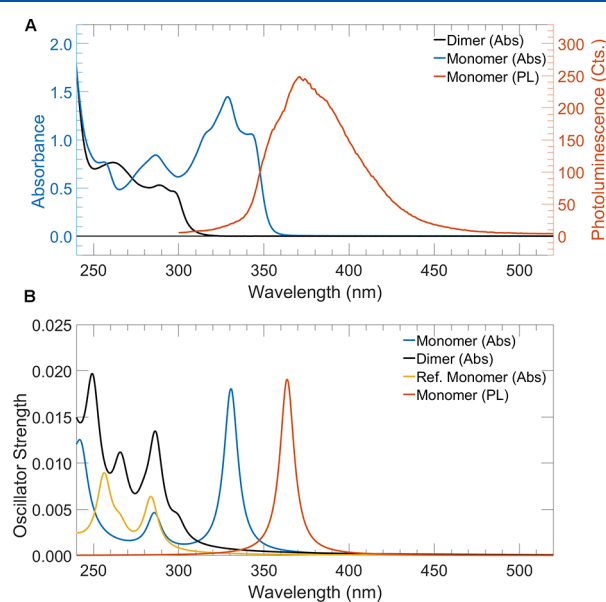


Figure 2. (A) Raw absorption (Abs) and emission spectra (PL) for the quinolinone dimer and monomers studied. (B) Calculated absorption spectra for the quinolinone monomer (blue trace), dimer (black trace), and reference monomer (ref. Monomer, yellow trace) which is devoid of the α,β double bond between carbons 3 and 4. Alongside is the calculated fluorescence spectrum of the quinolinone monomer (orange trace). Calculated spectra were obtained using TDA/TDDFT/CAM-B3LYP/6-31G* and shifted by -0.74 eV to compensate for missing solvation effects. The transitions are represented using Lorentzian curves and a full width at half-maximum of 10 nm.

(see also Figure S1 in the Supporting Information for comparison with the absorption spectra for the coumarin monomer and dimer studied previously¹⁹). Dimer stereochemical purity, following molecular synthesis, was checked by NOESY NMR (Figure S2), which showed the dimer to be isolated in the *syn-ht* stereoisomer. Consequently, the absorption spectrum relating to the quinolinone dimer is indicative of only the *syn-ht* stereoisomer. The dimer absorption (Figure 2A, black trace) from 240 nm onward shows significant absorption up until about 305 nm with an absorption onset of about 315 nm. By contrast, the quinolinone monomer (Figure 2A, blue trace) displays broader absorption extending until 350 nm with an onset at about 360 nm. The red-shifted absorption in the monomer arises from the extended π -conjugation across the carbon 3 and 4 positions. The same extension of the absorption to longer wavelengths has been observed for coumarin monomer systems. As with other known systems,¹⁵ single-photon cycloreversion of the dimer can occur when exposed to a short-wavelength photon, which in this system must be ≤ 315 nm. Likewise, irradiation of the monomer at wavelengths between 320 and 350 nm, resonant with the valence state, will lead to the cycloaddition reaction and accumulation of the dimerized photoproduct.⁴⁷ The photoluminescence spectrum of the quinolinone monomer is shown in Figure 2A. Attempts to measure the photoluminescence of the *syn-ht* quinolinone dimer stereoisomer were unsuccessful. Measurements showed only emission characteristic of the quinolinone monomer or nothing at all. We assigned observable, weak emission from the monomer as originating from degraded dimer in the sample and/or product formed from the actual photoluminescence experiment itself. The origin of this does not detract from the observation: emission from the dimer itself was not observed, and hence the dimer can be considered as nonemissive. The photoluminescence activity of unsubstituted coumarin is also known to be extremely low or practically nonemissive.^{48–50} In contrast, quinolinone monomer displayed a relative fluorescence quantum yield of $\approx 5\%$ in acetonitrile (see Figures S3–S4 for details), which is in accordance with previous literature.⁵¹

Quantum Chemical Calculations. Further insight into the fundamental electronic structure of the quinolinone monomer was obtained using quantum chemical calculations. The excitation energies for the lowest energy singlet and triplet states were calculated using a variety of computational methods (see Table S1). Inspection of the excitation energies and the intensities showed that, relative to the benchmark method of ADC(2), the less computationally demanding TDA/TDDFT/CAM-B3LYP agreed favorably and was used for further calculations. Thus, for the rest of this paper, all

Table 1. Calculated Vertical Excitation Energies (in eV) of the Energetically Lowest Singlet States of the Quinolinone Monomer, Dimer, and Reference Monomer^a

state	quinolinone monomer		quinolinone dimer		reference monomer	
	BHLYP	CAM-B3LYP	BHLYP	CAM-B3LYP	BHLYP	CAM-B3LYP
S ₁	4.64 (0.32)	4.49 (0.28) ($\pi\pi^*$)	5.08 (0.04)	4.88 (0.03)	5.32 (0.10)	5.11 (0.09)
S ₂	5.20 (0.05)	4.95 (0.00) ($n\pi^*$)	5.28 (0.17)	5.07 (0.17)	5.61 (0.07)	5.41 (0.03)
S ₃	5.30 (0.00)	5.08 (0.06) ($\pi\pi^*$)	5.30 (0.01)	5.09 (0.00)	5.77 (0.05)	5.58 (0.12)
S ₄	6.06 (0.14)	5.85 (0.12) ($\pi\pi^*$)	5.39 (0.04)	5.18 (0.03)	6.82 (0.23)	6.67 (0.47)
S ₅	6.47 (0.67)	6.33 (0.67) ($\pi\pi^*$)	5.57 (0.08)	5.38 (0.03)	6.95 (0.95)	6.71 (0.60)

^aOscillator strengths and characters for the S₀ → S_x transitions are given in parenthesis.

results are based on the TDA/TDDFT methods primarily using the CAM-B3LYP exchange-correlation functions. Electronic excitation energies were, subsequently, calculated for the quinolinone monomer, quinolinone dimer, and reference monomer subunit containing a π -electronic system more similar to one-half of the quinolinone dimer unit (see Figure S5). The excitation energies calculated for the three systems are given in Table 1. These values have been used in Figure 2B to generate theoretical absorption spectra. Continuing with the quinolinone monomer, the lowest excited state S_1 is of $\pi\pi^*$ character and is representative of the HOMO–LUMO transition corresponding to the bands at 315–350 nm. Due to the neglect of vibrational and solvation effects, the absolute values in Table 1 cannot be expected to perfectly match the experimental values.⁵² Additionally, it cannot be ruled out that the methods used can intrinsically generate over/underestimations of the energy levels based on approximations made within the physical models used. However, despite these issues, application of a constant offset of -0.74 eV to the values gives a very good agreement between the position of the calculated peaks and the average position of the bands in the raw absorption spectra.

A difference in results can be seen between use of the B3LYP and CAM-B3LYP basis functions. First, in all instances the B3LYP method gives more blue-shifted excitation energies than the CAM-B3LYP method. This suggests that the B3LYP method is more prone to overestimation of the excitation energies. Second, the next optically allowed transition is different in both methods. For the CAM-B3LYP method it is the S_3 state which is allowed, whereas the B3LYP predicts that the S_2 is optically allowed. Closer inspection of the calculated values in Table S1 shows that in general the CAM-B3LYP methods have a much more consistent offset from the experimental data, and hence it is used to reproduce the theoretical absorption spectra in Figure 2B. Assuming the CAM-B3LYP has more accurately resolved the locations of the valence transitions, from S_1 to S_3 , the S_2 state is an optically dark $n\pi^*$ transition, while the S_3 state is a weakly active $\pi\pi^*$ state. Furthermore, the emission spectrum was also simulated for the quinolinone monomer (Figure 2B and Table 2) using the same energetic shift and was found to agree very well with the position of the measured emission spectrum.

The lowest energy excited states of the quinolinone dimer, S_1 and S_2 , are blue-shifted with respect to the monomer, which shows the same trend observed in the raw spectra due to less π -conjugation. The S_1 and S_2 transitions are $\pi\pi^*$ in nature; however, the states are inherently mixed due to multiple orbital contributions. The reference monomer, which mimics one-half

Table 2. Calculated Vertical Emission Energies (in eV) of the Quinolinone Monomer (Right Column, S_1 (eq)) Compared with the Energies of Absorption (Left Column, S_0 (eq))^a

state	quinolinone monomer	
	S_0 (eq)	S_1 (eq)
S_1	4.49 (0.28)	4.15 (0.30)
S_2	4.95 (0.00)	4.74 (0.00)
S_3	5.08 (0.06)	4.89 (0.07)
S_4	5.85 (0.12)	5.72 (0.13)
S_5	6.33 (0.67)	6.22 (0.56)

^a $S_0 \rightarrow S_1$ oscillator strengths are quoted in parenthesis.

of the quinolinone dimer in terms of absolute π -conjugation, has calculated excitation energies that are all blue-shifted to higher energies than either the quinolinone dimer or monomer. This is interesting when comparing to the dimer, as it suggests that the quinolinone dimer π -systems, on each half of the molecule, exhibit through space electronic coupling.

Transient Absorption Spectroscopy. Before moving to the transient absorption (TA) data (Figure 3), we note that it

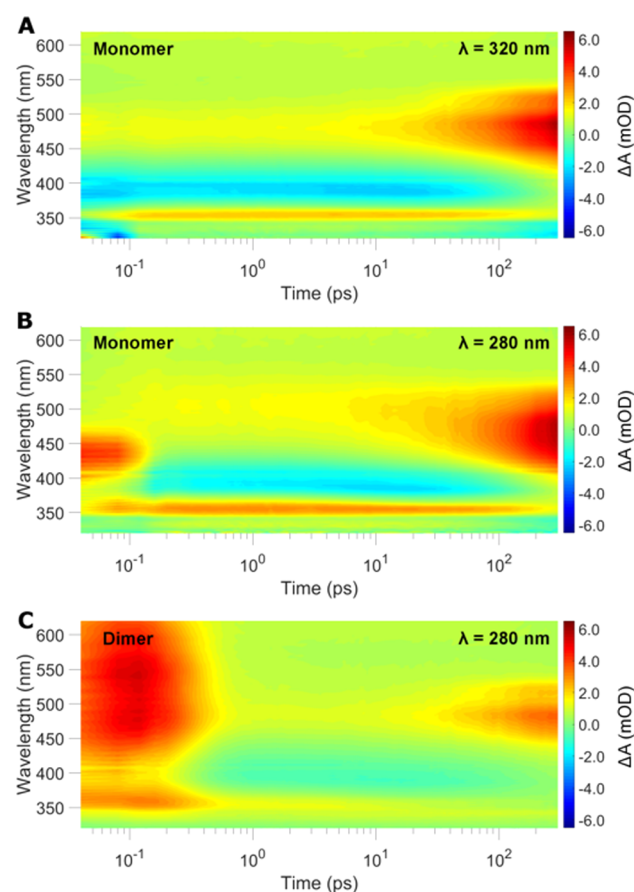


Figure 3. Surface plots of the transient absorption data for the quinolinone monomer and dimer: (A) quinolinone monomer excited at 320 nm; (B) quinolinone monomer excited at 280 nm; (C) quinolinone dimer excited at 280 nm. All samples were measured in acetonitrile.

was recently discovered that the photophysical behavior of both quinolinone systems differed substantially from the unsubstituted coumarins.^{19,49,50} A detailed comparison will be given in the Discussion section, but first we will describe the results of the quinolinone time-resolved spectroscopy. Starting with the quinolinone excited at 320 nm (Figure 3A), there are three main signals. The first dynamic feature, from time zero to 5 ps, is a set of signals consisting of a sharp excited state absorption (ESA) at 320–375 nm, stimulated emission (SE) at 375–430 nm, and a broad ESA from 430 to 620 nm. The SE signal matches the spontaneous emission in Figure 2A. After 5 ps the narrow ESA and SE underwent decay, while the broad ESA started to rise in positive amplitude over a period of 20–300 ps. For the monomer excited at 280 nm (Figure 3B), there is an additional ESA signal at 400–470 nm at times <0.2 ps, which after this time decays to zero leaving the same set of signals as seen in the monomer excited at 320 nm. Finally, the

quinolinone dimer excited at 280 nm (Figure 3C) shows an extremely broad ESA that spans the whole probe range and persists until 6–7 ps after which the data show clear signals reminiscent of photocleaved monomer in the excited singlet state.

Examination of the quinolinone monomer spectra (Figure 4A) and dynamics (Figure 4B) better describes the dynamics

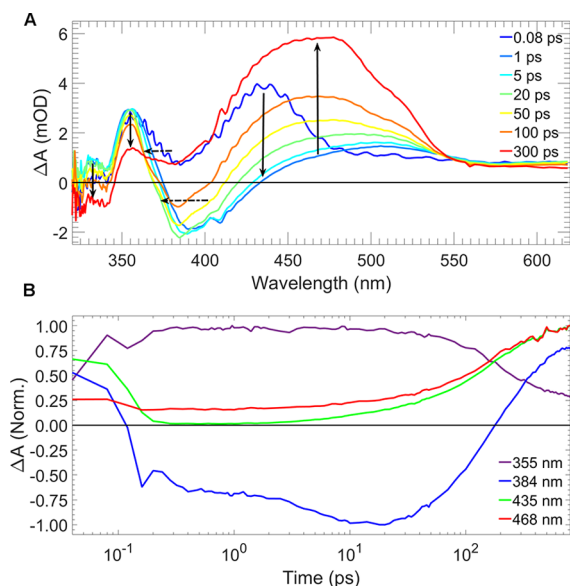


Figure 4. (A) Selected spectra for the quinolinone monomer excited at 280 nm. Time delays are indicated in the legend. Solid arrows are eye guides showing the direction of signal evolution/decay, and the dashed arrows are eye guides to emphasize the presence of spectral shifts. (B) Probe transients for the quinolinone monomer excited at 280 nm. Selected wavelengths are indicated in the legend.

quantitatively. Starting with the monomer spectra, the early-time subpicosecond ESA identified in Figure 3B is seen as the dark blue spectrum in Figure 4A at 80 fs, which is just after the instrument response of this measurement (ca. 60 fs). Within 0.2 ps this signal decays toward zero in the 370–460 nm spectral region and can be seen by looking at the 435 nm transient (Figure 4B, green). The rapid decay is characteristic of excitation to a higher lying singlet state. This is also apparent in the 384 nm transient (Figure 4B, blue), but in this case the signal inverts to negative amplitude as it is overlapped with the monomer SE band. From 0.1 to 150 ps the spectra display the negative SE peak, which is indicative of population of an emissive singlet state. Furthermore, the spectra undergo a shift to the blue across a period of ca. 20 ps (see Figure 4B, 384 nm transient). Finally, the data show the growth of a new absorbing species, as shown in the rise of the ESA across 380–530 nm. The 355 nm region appears to be indicative of mostly emissive singlet state as the transient shows a very constant behavior up until 30–40 ps when the signal starts to decay. It is at this time window where the longer time ESA begins to grow as shown in the 384, 435, and 468 nm transients (Figure 4B). Note that the 384 nm transient shows a greater rate of signal amplitude change, as it is a sum of the singlet SE decay and the growth of the longer time ESA signal. The origin of the longer time ESA was identified by long-time TA (Figures S6–S7) as that of a triplet state. Under aerobic conditions the lifetime of the triplet ESA was found to be 70 ns, but measurement using an argon purge to remove oxygen from the

sample resulted in an observable lifetime of 500 ns. The TA data for the quinolinone monomer excited at 320 nm are almost the same as in the 280 nm case with two exceptions. As is indicated in Figures 3A and 3B, the data for the 320 nm excitation show an absence of the short-time (<0.2 ps) ESA indicating a difference in singlet state population upon excitation. However, Figure 5 shows selected spectra for the

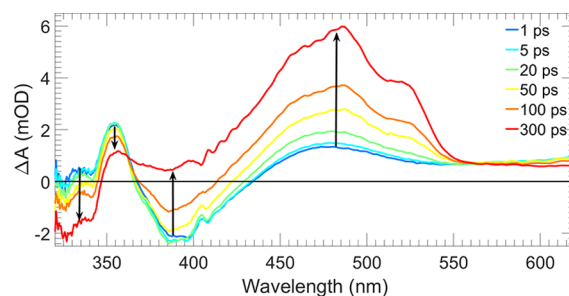


Figure 5. Selected TA spectra for the quinolinone monomer excited at 320 nm. Time intervals are indicated in the legend. Solid arrows are eye guides showing the direction of signal evolution/decay.

monomer excited at 320 nm, which also shows more clearly the absence or reduction in the presence of the blue-shift for the emissive singlet state signature. This absence of the spectral shift allows one to see the presence of an isosbestic point at 362 nm which is present due to the singlet to triplet intersystem crossing taking place.

Quinolinone dimers show a more drastic change in the TA data (see Figure 6). In the first 80 fs a broad ESA feature can

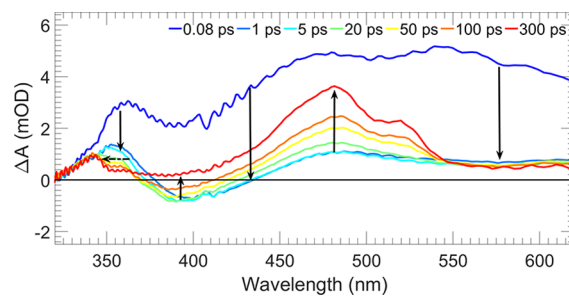


Figure 6. Selected TA spectra for the quinolinone dimer excited at 280 nm. Time intervals are indicated in the legend. Solid arrows are eye guides showing the direction of signal evolution/decay. The dashed arrow indicates a spectral shift.

be seen spanning the entire probed region. The ESA displays a noticeable minimum, or well, at the same position as the quinolinone monomer SE. By 1 ps, the ESA has decayed, and the TA signal looks highly reminiscent of the quinolinone monomer, exhibiting all the characteristic SE and ESA signatures seen previously. The only noticeable difference lies in the spectral region below 340 nm, where the signal shows a new ESA band which remains largely static with no obvious transient behavior. The data in this region are to be taken with a fair degree of uncertainty, as the supercontinuum probe used is particularly low in intensity, and therefore artifacts due to modulating pump–probe overlap and chromatic divergence in the probe may arise. For the remaining time range measured, the data follow that of the quinolinone monomer, displaying more fine structure in the spectra reminiscent of the monomer excited at 320 nm rather than at 280 nm.

Closer inspection of the data at the 320–360 nm range shows that there is relevant information present. At times from 100 to 300 ps, the signal at this range maintains a very constant amplitude and does not show signs of decay. Additionally, unlike both data sets for the quinolinone monomer, the data are completely positive in amplitude. Overlapping the TA spectra for the dimer at longer times of 100–400 ps and the monomer ground state absorption spectrum (Figure S8) shows that there is a similarity in the data; namely, the band edges for both sets match.

DISCUSSION

Assignment of the Transient Absorption Data. The data acquired for the quinolinone monomers, excited at the two different wavelengths, can be rationalized on the basis of three observable electronic states. Starting with the 280 nm data, the monomer is excited to a very short-lived singlet excited state, labeled in this paper as S_N . The S_N state is not indicative of the S_1 manifold. This is justified not only by its short lifetime but mainly due to its exclusive excitation with shorter wavelengths (280 nm). The assignment is further supported by the theoretical calculations, which predict that the two lowest energy optical transitions would be separated on the order of 0.59 eV (c.a. 4760 cm^{-1}). This energy separation matched that observed in the raw data, as the cluster of well-defined absorption peaks between 310 and 350 nm and a weaker band centered at 285 nm overlaps with the predicted optical excitation energies. Quantum chemical calculations propose that the origin of the higher energy, short-lived S_N state is the S_3 state, where the S_2 exhibits no appreciable optical cross section. Therefore, in the case of the 280 nm excitation, the rapid nonradiative relaxation is assigned to the transition from the S_3 state to the S_1 state. The subsequent blue-shift observed in the data from 1 to 20 ps is indicative of vibrational relaxation within the S_1 manifold. The lack of a blue-shift in the 320 nm data (Figure 3A and 5) reinforces this, as one would expect there to be population of multiple excited state vibrational levels upon population of the S_1 state from the S_3 relaxation process. Finally, the S_1 state exhibits a significant degree of intersystem crossing to the T_1 triplet manifold.

For the quinolinone dimer, the TA data is dominated in the short time (<1 ps) by an ESA originating from the dimer S_1 state (Figure 3C and 6). Following the decay of the dimer ESA, the resulting monomer TA spectra indicate that the dimer cleavage has formed monomer in the excited S_1 state. The cleavage from a 280 nm excitation can at most produce one monomer unit in the excited state as the input photon energy is less than twice the monomer S_1 singlet energy. The negative dip in the dimer ESA, as was noted previously, is in the same region as the monomer SE. This would suggest that upon excitation the dimer exciton couples to the monomer-pair intermediate state of one excited and one ground state in a very short period of time (<80 fs). Contaminant monomer present in the dimer sample, which would consequently give an artifact monomer TA signal, was ruled out as a possible cause as the samples were checked by UV/vis spectroscopy prior to measurement and only negligible amounts of monomer were found in the sample ($\ll 0.01$ OD background signal).

Global Target Analysis. In order to get more insight into the dynamics occurring in the quinolinone monomer and dimer system, a global target analysis was performed. Prior to the model development, SVD analysis was performed to give

an approximation of how many absorbing species there were for each system (Figures S9–S14). For the quinolinone dimer, four significant SVD eigenvalues were found, and therefore a model with four absorbing species was deduced. The model used for the dimer splitting is given in Figure 7. In summary,

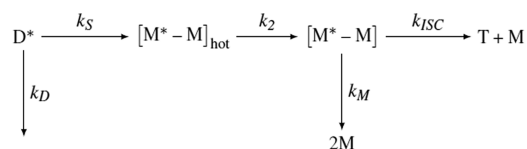


Figure 7. Model describing the quinolinone dimer ring cleavage. The excited state dimer, D^* , can undergo relaxation to the ground state (k_D) or split to form the vibrationally hot monomer ground–excited state product pair, $[M^* - M]$, where k_S is the rate of dimer splitting or ring cleavage. Subsequent vibrational relaxation occurs (k_2), and then either the relaxed monomer pair can undergo singlet relaxation, radiatively and nonradiatively (k_M), to form two monomers in the ground state or the excited state monomer can undergo intersystem crossing (k_{ISC}) to form the triplet state.

the kinetic model proposed has two branching points: one at the dimer excited state and one at the relaxed, vibrationally cold monomer product pair. Branching at the dimer excited state represents dimer relaxation to the ground state, given by k_D , and cleavage to the vibrationally hot monomer product pair, described by k_S . Control experiments (Figure S15–S16 and Table S2) showed that the quantum yield for the dimer ring cleavage was 0.23. With this value, it is possible to disentangle the two rate constants, k_D and k_S . The next step given by k_2 represents the vibrational cooling in both monomer units. We assume that both cooling rates are equivalent for the ground and excited state monomer units, and thus the difference spectra in the TA data have a 1:1 stoichiometric contribution from the monomer ground and excited states. The final step is the branching point at the vibrationally relaxed monomer pair, where k_M represents the radiative and nonradiative decay of the excited state monomer to the ground state and k_{ISC} is the rate of intersystem crossing. Unfortunately, without prior knowledge of either one of the rates or, for example the intersystem crossing yield, it is not possible to disentangle the two rates.

The model in Figure 7 predicts a three-exponential fit, but without full knowledge of the branching ratios it is not possible to directly determine the species-associated difference spectra (SADS). Instead, a triexponential fit was performed to give the decay-associated difference spectra (DADS) as shown in Figure 8A. The DADS are resolved to a combination of three transient spectra and one constant amplitude spectrum. By solving the set of differential equations (see the Supporting Information), which describe the mechanism in Figure 7, one can produce the time-dependent concentrations, and from there the evolution-associated difference spectra (EADS) can be extracted (Figure 8B). The EADS map the transient spectra of all species evolving with the same dynamics. Note that the dimer excited state is the only pure spectral signature. All other components are mixtures of either the vibrationally hot and cold excited and ground state monomers and the triplet–monomer pair. The contribution of the partners to each EADS is 1:1 by mass balance. However, with no information as to the absorption coefficients of each, it is not possible to disentangle the mixed state spectra into individual components.

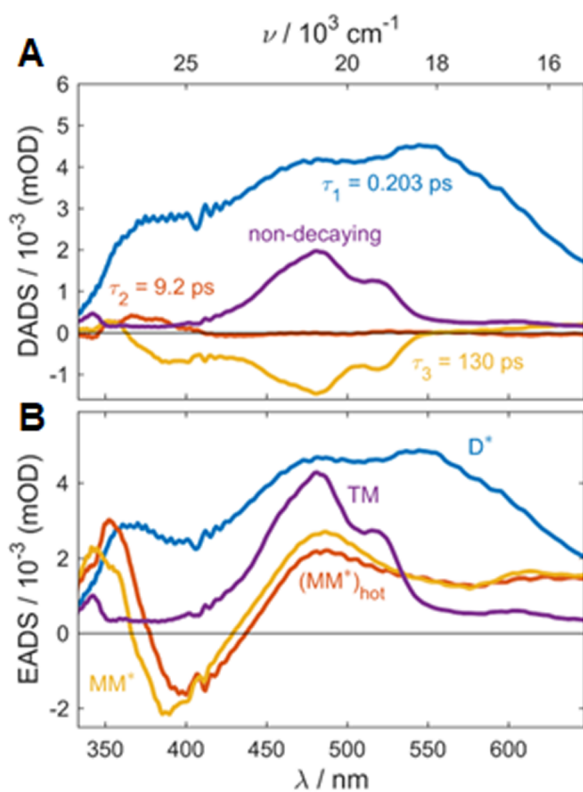


Figure 8. (A) Decay-associated difference spectra (DADS) of the quinolinone dimer excited at 280 nm. (B) Evolution-associated difference spectra (EADS) of the dimer excited at 280 nm.

The computed EADS spectra display good agreement with what one would predict by empirical observation of the raw TA data. The dimer excited state (Figure 8B blue trace) shows the broad ESA feature with the dip at the region around 400 nm, which indicates possible presence of already cleaved quinolinone monomer in the singlet excited state. This in turn indicates that the initial step from dimer to the heterogeneous monomer product pair already occurs with substantial weight within the 200 fs regime. The computed inverse rate constant for this step was found to be 203 fs. Note that here we use the term heterogeneous as a reference to the differing electronic states between the two monomers formed immediately after cleavage; namely, one is in a ground singlet state, and one is in an excited singlet state. The second and third species in the EADS are the vibrationally hot and relaxed, heterogeneous monomer product pair, respectively. The EADS for these species are spectrally shifted, which is in accordance with that observed in the raw data for both the quinolinone monomer and dimer systems. The spectral shift, as stated previously, represents the process of vibrational cooling within the singlet states. For the dimer, since it is not possible to disentangle the individual contributions of the ground state and excited singlet state monomers we assume that the cooling proceeds in both monomers with the same rate. The process is estimated to occur with an inverse rate constant of 9.2 ps. Within the two monomer EADS spectra computed for the dimer data, there is also the presence of the ground state monomer absorption at the wavelength regime below 360 nm. Finally, the EADS for the triplet state is computed with good agreement to the raw data. The number obtained from the global fit, of 130 ps, is representative of the monomer singlet lifetime and not the inverse rate of intersystem crossing. Without prior knowledge

of the singlet to triplet intersystem crossing quantum yield, this number cannot be deduced. However, empirical inspection of the raw data suggests that, based purely on the magnitude of the singlet and triplet signatures, the intersystem crossing yield may be on the order of 50% compared to the total singlet decay, both nonradiatively and radiatively. This would put the inverse rate of intersystem crossing on the order of twice the value computed for the singlet lifetime. The results of the global analysis for the quinolinone monomer are shown in the Supporting Information (Figures S17–19). The results were found to be in good agreement with the dimer system. The resolved EADS and the extrapolated rate constant for the vibrational relaxation within the excited monomer singlet state were found to match particularly well with that found in the dimer.

Comparison of Quinolinone Dynamics to Coumarin.

The results for the quinolinone monomer and dimer species display substantial differences to that observed for the corresponding coumarin systems studied previously.^{19,49} To start with the monomers, the quinolinone displays more emission ($\approx 5\%$ fluorescence quantum yield) than the unsubstituted coumarin, which by comparison is nonemissive.^{49,53} The coumarin also shows no appreciable triplet yield, within the same solvent conditions, whereas the quinolinone shows substantial triplet formation. Control experiments using 7-methoxycoumarin and 7-hydroxycoumarin (umbelliferone), given in Figures S20–S21, which have the same phenyl ring functionalization making them more structurally similar to the quinolinones, were performed. The data showed that both control compounds were emissive, but no appreciable quantity of triplet ESA was observed despite the similar decay time of the S_1 state. This indicates that the methoxy functionalization is the primary structure–function control that governs the increase in radiative quantum yield. This observation is in accordance with the literature around emissive coumarins as, e.g., laser dyes, where one of the key synthetic controls is to functionalize the coumarin with electron-donating groups at the 7-carbon position, and this is particularly effective when the electronegative functional group is amine based.⁵³ However, the lack of triplet ESA in the control coumarins indicates that the dominating structural unit controlling the presence or absence of intersystem crossing is the lactame unit. The substitution of an oxygen to a nitrogen, as is the case when converting from a lactone to a lactame, is a simple case of altering the degree of spin–orbit coupling in organic systems that lack heavy atoms. Such phenomena is in accordance with El-Sayed’s rule.⁵⁴

For the dimer cleavage, a schematic summarizing the two different pathways is given in Figure 9. Additionally, for a more physically relevant expression of the system, a Jablonski diagram has been constructed based on the all the data obtained and is shown with description in Figure S22. Coumarin dimers were found to undergo a more homogeneous ring cleavage, whereby the resulting monomer products were formed exclusively in the ground singlet state but in a vibrationally hot state with subsequent vibrational cooling. By contrast, the quinolinones display the heterogeneous pathway whereby one monomer is formed in the first excited singlet state and the other is in the ground state with a lesser degree of vibrational cooling, but it is still present. Within the experimental temporal resolution, it is not possible to unambiguously establish whether the heterogeneous mechanism found for the quinolinones is exclusive or a homogeneous

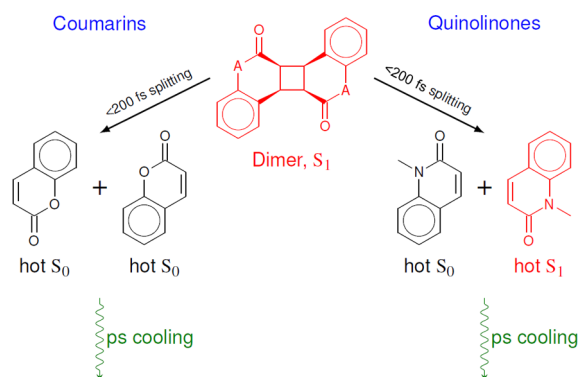


Figure 9. Schematic showing the two different splitting mechanisms found when studying coumarin and quinolinone dimer ring cleavage.

channel contributes to a small degree. To resolve this question would require that a far more quantitative experiment is needed, where the contribution of excited state monomer signal can be referenced to the total amount of initial dimer excited states formed. When factoring in the intrinsic quantum yield of dimer ring cleavage, results that deviate significantly from a ratio of 1:1 dimer signal to excited state monomer signal would indicate a mixture of heterogeneous and homogeneous ring cleavage pathways present.

CONCLUSION

To summarize, we have measured a new class of compounds based on the traditionally studied coumarin-based systems and found substantial changes were made to the reaction coordinate for dimer ring cleavage. Substitution of the lactone unit in classical coumarins for a lactame unit, transforming the molecule into a quinolinone framework, has been demonstrated to radically alter the photophysical properties of both monomer and dimer species. This discovery of the ability to alter the intersystem crossing yield in such a way for this class of compounds has several potential ramifications. The quinolinones were found to have intrinsically higher yields for dimerization reactions compared to the coumarin counterparts. The classic coumarin dimerization reaction is believed to proceed via the triplet state primarily due to diffusional rate limitations. Subsequently, it makes sense based on the data within this paper why relatively unsubstituted quinolinones display a higher tendency to dimerize. Additionally, quinolinones with their higher intrinsic yield of triplet formation could be more useful in, for example, dimer-based polymer cross-linking and solid-state polymer synthesis. For the dimers, detailed quantum chemical studies will be needed to give first insights into how the nature of the carbonyl group changes the potential energy landscape and how it dictates the monomer product distribution. There are a few interesting applications and ramifications of this discovery that can be considered. For drug delivery systems, the enhanced ring cleavage efficiency alone makes quinolinones more desirable as light-activated medical agents than coumarins. Production of monomer in the singlet state may be useful in chromatically selective activation of fluorescent probe for medical imaging purposes. To elucidate with a hypothetical example, 7-aminocoumarins tend to have very high fluorescent quantum yields. Assuming the effect is similar for 7-aminoquinolinones or use of some modified quinolinone with a high fluorescence yield, one could imagine fluorescent inactive quinolinone dimers that become

fluorescence active only after the UV-induced ring cleavage process has occurred. For synthetic purposes, the intrinsically higher ISC of the quinolinone monomers explains, in part, why the reaction times for dimer formation are substantially shorter than in coumarins, making the synthetic procedure more efficient.

ASSOCIATED CONTENT

Supporting Information

The Supporting Information is available free of charge on the ACS Publications website at DOI: 10.1021/acs.jpca.8b07186.

Fluorescence and absorption spectra used for the fluorescence quantum yield derivation, selected spectra and kinetics from the transient absorption data, singular value decomposition analysis of the data, population dynamics, nanosecond transient absorption of the quinolinones, table of excitation energies computed for the quinolinone monomer with a range of methodologies, data for the dimer cleavage quantum yield determination, structural model of the reference monomer calculated, and fs–ps transient absorption of various functionalized coumarin control molecule (PDF)

AUTHOR INFORMATION

Corresponding Authors

*E-mail: hampp@uni-marburg.de.

*E-mail: marcus.motzkus@pci.uni-heidelberg.de.

ORCID

Tiago Buckup: 0000-0002-1194-0837

Andreas Dreuw: 0000-0002-5862-5113

Norbert Hampp: 0000-0003-1614-2698

Author Contributions

N.P., M.J., N.H., and M.M. conceived the experiment and project. N.B. synthesized the compounds and carried out dimerization efficiency experiments. M.J., N.W., Y.L., and J.L.P.L. performed the transient absorption measurements. N.P. performed fluorescence quantum yield measurements, developed the global analysis methods, and analyzed the transient absorption data. N.P., T.B., J.L.P.L., and M.M. reviewed and discussed the data. A.D. performed the computational calculations. N.P., T.B., J.L.P.L., and M.M. reviewed and wrote the paper

Notes

The authors declare no competing financial interest.

ACKNOWLEDGMENTS

We gratefully acknowledge support by the Deutsche Forschungsgemeinschaft (DFG, Sonderforschungsbereich SFB 1249, TP B4).

REFERENCES

- (1) Satyapal, S.; Park, J.; Bersohn, R.; Katz, B. Dissociation of Methanol and Ethanol Activated by a Chemical Reaction or by Light. *J. Chem. Phys.* **1989**, *91*, 6873.
- (2) Fagnoni, M.; Dondi, D.; Ravelli, D.; Albini, A. Photocatalysis for the Formation of the C-C Bond. *Chem. Rev.* **2007**, *107*, 2725–2756.
- (3) Liebel, M.; Schnedermann, C.; Kukura, P. Vibrationally Coherent Crossing and Coupling of Electronic States during Internal Conversion in β -Carotene. *Phys. Rev. Lett.* **2014**, *112*, 1–5.

- (4) Szarka, A. Z.; Pugliano, N.; Palit, D. K.; Hochstrasser, R. M. Vibrational Coherence in the Solution Phase Photoisomerization Reaction of Cis-Stilbene. *Chem. Phys. Lett.* **1995**, *240*, 25–30.
- (5) Clark, J.; Nelson, T.; Tretiak, S.; Cirmi, G.; Lanzani, G. Femtosecond Torsional Relaxation. *Nat. Phys.* **2012**, *8*, 225–231.
- (6) Douhal, A.; Kim, S. K.; Zewail, A. H. Femtosecond Molecular Dynamics of Tautomerization in Model Base Pairs. *Nature* **1995**, *378*, 260–263.
- (7) Andradý, A. L.; Hamid, S. H.; Hu, X.; Torikai, A. Effects of Increased Solar Ultraviolet Radiation on Materials. *J. Photochem. Photobiol., B* **1998**, *46*, 96–103.
- (8) Alger, R. S.; Anderson, T. H.; Webb, L. A. Irradiation Effects in Simple Organic Solids. *J. Chem. Phys.* **1959**, *30*, 695.
- (9) Rumora, A. E.; Kolodziejczak, K. M.; Malhowski Wagner, A.; Núñez, M. E. Thymine Dimer-Induced Structural Changes to the DNA Duplex Examined with Reactive Probes †. *Biochemistry* **2008**, *47*, 13026–13035.
- (10) Schreier, W. J.; Schrader, T. E.; Koller, F. O.; Gilch, P.; Crespo-Hernandez, C. E.; Swaminathan, V. N.; Carell, T.; Zinth, W.; Kohler, B. Thymine Dimerization in DNA Is an Ultrafast Photoreaction. *Science* **2007**, *315*, 625–629.
- (11) Dulić, D.; van der Molen, S. J.; Kudernac, T.; Jonkman, H. T.; de Jong, J. J. D.; Bowden, T. N.; van Esch, J.; Feringa, B. L.; van Wees, B. J. One-Way Optoelectronic Switching of Photochromic Molecules on Gold. *Phys. Rev. Lett.* **2003**, *91*, 207402.
- (12) Tian, H.; Yang, S. Recent Progresses on Diarylethene Based Photochromic Switches. *Chem. Soc. Rev.* **2004**, *33*, 85–97.
- (13) Feringa, B. L. Control of Motion: From Molecular Switches to Molecular Motors. *Acc. Chem. Res.* **2001**, *34*, 504–513.
- (14) Behrendt, P. J.; Kim, H. C.; Hampp, N. Photochemical Cleavage of Individual Stereoisomers of Coumarin-5-Fluorouracil Crossdimers via Single- and Two-Photon-Absorption. *Chem. Phys. Lett.* **2013**, *588*, 91–96.
- (15) Backup, T.; Southan, A.; Kim, H. C.; Hampp, N.; Motzkus, M. Optimisation of Two-Photon Induced Cleavage of Molecular Linker Systems for Drug Delivery. *J. Photochem. Photobiol., A* **2010**, *210*, 188–192.
- (16) Kim, H. C.; Härtner, S.; Hampp, N. Single- and Two-Photon Absorption Induced Photocleavage of Dimeric Coumarin Linkers: Therapeutic versus Passive Photocleavage in Ophthalmologic Applications. *J. Photochem. Photobiol., A* **2008**, *197*, 239–244.
- (17) Härtner, S.; Kim, H. C.; Hampp, N. Photodimerized 7-Hydroxycoumarin with Improved Solubility in PMMA: Single-Photon and Two-Photon-Induced Photocleavage in Solution and PMMA Films. *J. Photochem. Photobiol., A* **2007**, *187*, 242–246.
- (18) Kim, H.-C.; Härtner, S.; Behe, M.; Behr, T. M.; Hampp, N. A. Two-Photon Absorption-Controlled Multidose Drug Release: A Novel Approach for Secondary Cataract Treatment. *J. Biomed. Opt.* **2006**, *11*, 034024.
- (19) Jiang, M.; Paul, N.; Bieniek, N.; Backup, T.; Hampp, N.; Motzkus, M. Photocleavage of Coumarin Dimers Studied by Femtosecond UV Transient Absorption Spectroscopy. *Phys. Chem. Chem. Phys.* **2017**, *19*, 4597–4606.
- (20) Backup, T.; Dorn, J.; Hauer, J.; Härtner, S.; Hampp, N.; Motzkus, M. The Photoinduced Cleavage of Coumarin Dimers Studied with Femtosecond and Nanosecond Two-Photon Excitation. *Chem. Phys. Lett.* **2007**, *439*, 308–312.
- (21) Kim, H.-C.; Kreiling, S.; Greiner, A.; Hampp, N. Two-Photon-Induced Cycloreversion Reaction of Coumarin Photodimers. *Chem. Phys. Lett.* **2003**, *372*, 899–903.
- (22) Yonezawa, N.; Yamashita, T.; Kano, T.; Saigo, T.; Hasegawa, M. Application of Anisotropic Photocleavage of Head-To-Head Type Cyclobutane Compounds. *Ind. Eng. Chem. Prod. Res. Dev.* **1985**, *24*, 593–598.
- (23) Yonezawa, N.; Yoshida, T.; Hasegawa, M. Symmetric and Asymmetric Photocleavage of the Cyclobutane Rings in Head-to-Head Coumarin Dimers and Their Lactone-Opened Derivatives. *J. Chem. Soc., Perkin Trans. 1* **1983**, *1*, 1083–1086.
- (24) Wolff, T.; Görner, H. Photocleavage of Dimers of Coumarin and 6-Alkylcoumarins. *J. Photochem. Photobiol., A* **2010**, *209*, 219–223.
- (25) Helmstetter, S.; Badur, T.; Hampp, N. High-Refractive Quinolinone-Based Polymers for Ophthalmic Devices. *J. Polym. Res.* **2016**, *23*, 1–14.
- (26) Patel, M.; McHugh, R. J.; Cordova, B. C.; Klabe, R. M.; Bachelier, L. T.; Erickson-Viitanen, S.; Rodgers, J. D. Synthesis and Evaluation of Novel Quinolinones as HIV-1 Reverse Transcriptase Inhibitors. *Bioorg. Med. Chem. Lett.* **2001**, *11*, 1943–1945.
- (27) Hradil, P.; Hlavac, J.; Soural, M.; Hajduch, M.; Kolar, M.; Vecerova, R. 3-Hydroxy-2-Phenyl-4(1H)-Quinolinones as Promising Biologically Active Compounds. *Mini-Rev. Med. Chem.* **2009**, *9*, 696–702.
- (28) Barraja, P.; Diana, P.; Montalbano, A.; Dattolo, G.; Cirrincione, G.; Viola, G.; Vedaldi, D.; Dall'Acqua, F. Pyrrolo[2,3-H]quinolinones: A New Ring System with Potent Photoantiproliferative Activity. *Bioorg. Med. Chem.* **2006**, *14*, 8712–8728.
- (29) Tedesco, R.; Shaw, A. N.; Bambal, R.; Chai, D.; Concha, N. O.; Darcy, M. G.; Dhanak, D.; Fitch, D. M.; Gates, A.; Gerhardt, W. G.; et al. 3-(1,1-Dioxo-2H-(1,2,4)-Benzothiadiazin-3-Yl)-4-Hydroxy-2(1H)-Quinolinones, Potent Inhibitors of Hepatitis C Virus RNA-Dependent RNA Polymerase. *J. Med. Chem.* **2006**, *49*, 971–983.
- (30) Wang, T.-C.; Chen, Y.-L.; Lee, K.-H.; Tzeng, C.-C. Lewis Acid Catalyzed Reaction of Cinnamylidides: Competition of Intramolecular and Intermolecular Friedel-Crafts Reaction. *Synthesis* **1997**, *1997*, 87–90.
- (31) Kozma, I.; Baum, P.; Lochbrunner, S.; Riedle, E. Widely Tunable Sub-30 Fs Ultraviolet Pulses by Chirped Sum Frequency Mixing. *Opt. Express* **2003**, *11*, 3110–3115.
- (32) Manzoni, C.; Polli, D.; Cerullo, G. Two-Color Pump-Probe System Broadly Tunable over the Visible and the near Infrared with Sub-30 Fs Temporal Resolution. *Rev. Sci. Instrum.* **2006**, *77*, 023103.
- (33) Baum, P.; Lochbrunner, S.; Riedle, E. Tunable Sub-10-Fs Ultraviolet Pulses Generated by Achromatic Frequency Doubling. *Opt. Lett.* **2004**, *29*, 1686–1688.
- (34) Baum, P.; Lochbrunner, S.; Riedle, E. Generation of Tunable 7-Fs Ultraviolet Pulses: Achromatic Phase Matching and Chirp Management. *Appl. Phys. B: Lasers Opt.* **2004**, *79*, 1027–1032.
- (35) Kovalenko, S. A.; Dobryakov, A. L.; Ruthmann, J.; Ernsting, N. P. Femtosecond Spectroscopy of Condensed Phases with Chirped Supercontinuum Probing. *Phys. Rev. A: At., Mol., Opt. Phys.* **1999**, *59*, 2369–2384.
- (36) Becke, A. D. Density-Functional Thermochemistry. III. The Role of Exact Exchange. *J. Chem. Phys.* **1993**, *98*, 5648–5652.
- (37) Grimme, S.; Antony, J.; Ehrlich, S.; Krieg, H. A Consistent and Accurate Ab Initio Parametrization of Density Functional Dispersion Correction (DFT-D) for the 94 Elements H-Pu. *J. Chem. Phys.* **2010**, *132*, 154104.
- (38) Dreuw, A.; Head-Gordon, M. Single-Reference Ab Initio Methods for the Calculation of Excited States of Large Molecules. *Chem. Rev.* **2005**, *105*, 4009–4037.
- (39) Hirata, S.; Head-Gordon, M. Time-Dependent Density Functional Theory within the Tamm–Dancoff Approximation. *Chem. Phys. Lett.* **1999**, *314*, 291–299.
- (40) Shao, Y.; Head-Gordon, M.; Krylov, A. I. The Spin-Flip Approach within Time-Dependent Density Functional Theory: Theory and Applications to Diradicals. *J. Chem. Phys.* **2003**, *118*, 4807–4818.
- (41) Yanai, T.; Tew, D. P.; Handy, N. C. A New Hybrid Exchange-Correlation Functional Using the Coulomb-Attenuating Method (CAM-B3LYP). *Chem. Phys. Lett.* **2004**, *393*, 51–57.
- (42) Head-Gordon, M.; Rico, R. J.; Oumi, M.; Lee, T. J. A Doubles Correction to Electronic Excited States from Configuration Interaction in the Space of Single Substitutions. *Chem. Phys. Lett.* **1994**, *219*, 21–29.
- (43) Schirmer, J. Beyond the Random-Phase Approximation: A New Approximation Scheme for the Polarization Propagator. *Phys. Rev. A: At., Mol., Opt. Phys.* **1982**, *26*, 2395–2416.

(44) Wormit, M.; Rehn, D. R.; Harbach, P. H. P.; Wenzel, J.; Krauter, C. M.; Epifanovsky, E.; Dreuw, A. Investigating Excited Electronic States Using the Algebraic Diagrammatic Construction (ADC) Approach of the Polarisation Propagator. *Mol. Phys.* **2014**, *112*, 774–784.

(45) Dreuw, A.; Wormit, M. The Algebraic Diagrammatic Construction Scheme for the Polarization Propagator for the Calculation of Excited States. *Wiley Interdiscip. Rev. Comput. Mol. Sci.* **2015**, *5*, 82–95.

(46) Shao, Y.; Gan, Z.; Epifanovsky, E.; Gilbert, A. T. B.; Wormit, M.; Kussmann, J.; Lange, A. W.; Behn, A.; Deng, J.; Feng, X.; et al. Advances in Molecular Quantum Chemistry Contained in the Q-Chem 4 Program Package. *Mol. Phys.* **2015**, *113*, 184–215.

(47) Trenor, S. R.; Shultz, A. R.; Love, B. J.; Long, T. E. Coumarins in Polymers: From Light Harvesting to Photo-Cross-Linkable Tissue Scaffolds. *Chem. Rev.* **2004**, *104*, 3059–3078.

(48) Hoffman, R.; Wells, P.; Morrison, H. Organic Photochemistry. XII. Further Studies on the Mechanism of Coumarin Photo-dimerization. Observation of an Unusual “Heavy Atom” Effect. *J. Org. Chem.* **1971**, *36*, 102–108.

(49) Krauter, C. M.; Möhring, J.; Backup, T.; Pernpointner, M.; Motzkus, M. Ultrafast Branching in the Excited State of Coumarin and Umbelliferone. *Phys. Chem. Chem. Phys.* **2013**, *15*, 17846–17861.

(50) Murdock, D.; Ingle, R. A.; Sazanovich, I. V.; Clark, I. P.; Harabuchi, Y.; Taketsugu, T.; Maeda, S.; Orr-Ewing, A. J.; Ashfold, M. N. R. Contrasting Ring-Opening Propensities in UV-Excited α -Pyrone and Coumarin. *Phys. Chem. Chem. Phys.* **2016**, *18*, 2629–2638.

(51) Fabian, W. M. F.; Niederreiter, K. S.; Uray, G.; Stadlbauer, W. Substituent Effects on Absorption and Fluorescence Spectra of Carbostyryls. *J. Mol. Struct.* **1999**, *477*, 209–220.

(52) Klamt, A. Calculation of UV/Vis Spectra in Solution. *J. Phys. Chem.* **1996**, *100*, 3349–3353.

(53) Kuznetsova, N. A.; Kaliya, O. L. The Photochemistry of Coumarins. *Russ. Chem. Rev.* **1992**, *61*, 683–696.

(54) Baba, M. Intersystem Crossing in the $1\text{N}\pi^*$ and $1\text{I}\pi^*$ States. *J. Phys. Chem. A* **2011**, *115*, 9514–9519.